HHS Public Access

Author manuscript

Cell Rep. Author manuscript; available in PMC 2019 October 21.

Published in final edited form as:

Cell Rep. 2018 November 13; 25(7): 1708–1717.e5. doi:10.1016/j.celrep.2018.10.040.

Autophagy Ablation in Adipocytes Induces Insulin Resistance and Reveals Roles for Lipid Peroxide and Nrf2 Signaling in Adipose-Liver Crosstalk

Jinjin Cai[1], **Karla M. Pires**[2], **Maroua Ferhat**[2], **Bhagirath Chaurasia**[2], **Ma´rcio A. Buffolo**[2], **Rana Smalling**[1], **Ashot Sargsyan**[1], **Donald L. Atkinson**[2], **Scott A. Summers**[2], **Timothy E. Graham**[1,3,*], **Sihem Boudina**[2,4,*]

[1]Division of Endocrinology Diabetes and Metabolism, University of Utah School of Medicine, Salt Lake City, UT 84112, USA

[2]Department of Nutrition and Integrative Physiology, University of Utah College of Health and Program in Molecular Medicine, Salt Lake City, UT 84112, USA

[3]Progenitor Life Sciences, Salt Lake City, UT 84108, USA

[4]Lead Contact

SUMMARY

Autophagy is a homeostatic cellular process involved in the degradation of long-lived or damaged cellular components. The role of autophagy in adipogenesis is well recognized, but its role in mature adipocyte function is largely unknown. We show that the autophagy proteins Atg3 and Atg16L1 are required for proper mitochondrial function in mature adipocytes. In contrast to previous studies, we found that post-developmental ablation of autophagy causes peripheral insulin resistance independently of diet or adiposity. Finally, lack of adipocyte autophagy reveals cross talk between fat and liver, mediated by lipid peroxide-induced Nrf2 signaling. Our data reveal a role for autophagy in preventing lipid peroxide formation and its transfer in insulin-sensitive peripheral tissues.

In Brief

Cai et al. describe how lack of autophagy in mature adipocytes causes insulin resistance with no change in body weight. Adipocytes lacking Atg3 or Atg16L1 accumulate dysfunctional mitochondria and have increased lipid peroxidation and Nrf2 and keap1 activation. This study reveals a role for lipid peroxides and Nrf2 signaling in an adipose-liver crosstalk.

*Correspondence: tim.graham@progenitorlifesciences.com (T.E.G.), sihem.boudina@u2m2.utah.edu (S.B.).

AUTHOR CONTRIBUTIONS

J.C., K.M.P., M.F., B.C., M.A.B., R.S., A.S., and D.L.A. designed and performed experiments. S.A.S. edited the manuscript. S.B. designed experiments, interpreted data, and wrote the manuscript. T.E.G. conceived and designed the project, interpreted data, and edited the manuscript. S.B. is responsible for the integrity of the content.

DECLARATION OF INTERESTS

The authors declare no competing interests.

SUPPLEMENTAL INFORMATION

Supplemental Information includes four figures and two tables and can be found with this article online at https://doi.org/10.1016/j.celrep.2018.10.040.

Graphical Abstract

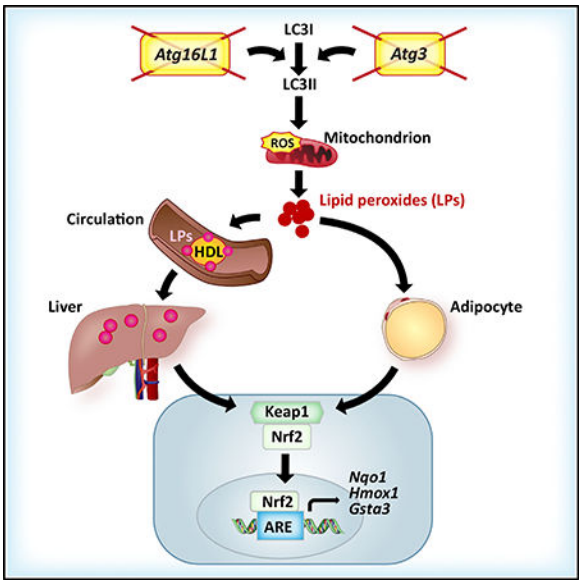

INTRODUCTION

Optimal function of white and brown adipose tissues is critical for controlling nutrient homeostasis and maintaining metabolic health. Adipocytes of white adipose tissue (WAT) store fatty acids and glucose as triglycerides, whereas a dipocytes of brown adipose tissue (BAT) oxidize lipids and glucose to generate body heat (thermogenesis). WAT also contains beige adipocytes with a similar thermogenic function. Poised at the fulcrum between fuel storage and utilization, adipocytes also play an important role in sensing nutritional and energetic states of the organism and continuously communicate with other tissues via a variety of signals—both neural and endocrine—to coordinate metabolism throughout the body. Aberrant communication between adipocytes and other tissues (e.g., brain, liver, and muscle) leads to diseases such as obesity and diabetes and is additionally implicated in cardiovascular disease (CVD) and cancer. Hence, establishing mechanisms by which adipocytes broadcast systemic messages to other tissues has been an important focus of metabolic research.

Macroautophagy (referred to here as autophagy) removes old or damaged cellular material, including protein aggregates, oxidized lipids, and organelles, from cells (Mizushima, 2007). Autophagy plays a particularly important role in maintaining the mitochondrial health of cells by removing aged or damaged mitochondria, especially those capable of producing dangerous levels of reactive oxygen species (ROS) (Novak, 2012). Moreover, prior studies indicate that autophagy markers are elevated in adipose tissue of obese humans (Jansen et al., 2012; Kosacka et al., 2013; Ost et al., 2010). Nevertheless, the role of autophagy in adipocyte function is largely unknown. Prior efforts to study adipocyte autophagy made use of mouse models in which autophagy was inhibited at early stages of development. Although this work revealed critical and unexpected roles for autophagy in adipocyte development, it could not elucidate the normal function of autophagy in mature adipocytes

because the mice lacking autophagy in these models could not produce fully differentiated adipocytes and failed to form normal WAT depots. To explore the function of autophagy in white and brown adipocytes, we generated mice in which key components of the autophagy system—Atg3 and Atg16L1—can be subjected to genetic KO in a temporally controlled fashion, making it possible to study the effects of inhibiting autophagy in fully differentiated adipocytes of adult mice *in vivo*.

Our findings indicate that post-developmental impairment of autophagy leads to dysfunctional mitochondria, adipose inflammation, and whole-body insulin resistance. The condition is characterized by accumulation of lipid peroxides and induction of oxidant detoxification genes in the Nrf2 and Keap1 signaling network. Surprisingly, some of the adipocyte-derived lipid peroxides appear to traffic, via circulating high-density lipoproteins (HDLs), to the liver, leading to Nrf2 and Keap1 activation in that tissue as well. These data uncover a fundamental role for autophagy in suppressing oxidative injury within the adipocyte and present a signaling mechanism by which adipose damage influences liver function and peripheral insulin sensitivity.

RESULTS AND DISCUSSION

Depletion of Atg3 or Atg16L1 Reduces Autophagic Flux in Brown and WAT

We established two mouse models that enable temporally controlled inhibition of autophagy in mature adipocytes. Briefly, 1708 Cell Reports 25, 1708–1717, November 13, 2018 [a] 2018 University of Utah. This is an open access article under the CC BY-NC-ND license (http://creativecommons.org/licenses/by-nc-nd/4.0/). we engineered two independent lines of mice harboring loxP sites in critical exons of the genes Atg3 and Atg16L1. We chose to target Atg3 and Atg16L1 because of their important role in LC3 conjugation system. Indeed, Atg3 and Atg16L1 are required for LC3 lipidation, a step necessary for autophagosome maturation (Fujita et al., 2008; Sou et al., 2008). The floxed lines were bred to mice carrying a tamoxifen-inducible CreER^{T2} transgene under the control of the adiponectin promoter (*Adipoq*-CreER^{T2}) (Sassmann et al., 2010). These animals and non-floxed controls were treated with tamoxifen starting at 8 weeks of age. As expected, this intervention depleted Atg3 and Atg16L1 proteins in WAT and in BAT, but not in other tissues were examined (Figures 1A–1D and S1A–S1H). The resulting Atg3 knockout (AdiAtg3KO) and Atg16L1 knockout (AdiAtg16L1KO) mice exhibited marked reductions in autophagic flux both in white and brown depots, as evidenced by a substantial reduction in LC3I lipidation to LC3II (Figures 1A–1D and S1E–S1H). The impairment in autophagy also led to the accumulation of the adaptor proteins p62 or Sqstm1 and Nbr1, two known targets of the autophagic machinery (Kirkin et al., 2009; Pankiv et al., 2007), in WAT and BAT but not in other tissues (Figures 1A–1D and S1A–S1H). These data strongly support the utility of these models for studying loss of autophagy in mature adipocytes of adult mice.

Post-Developmental Depletion of Atg3 and/or Atg16L1 Increases Adipose Tissue Inflammation without Affecting Body Weight or Composition

We monitored body weight and composition in AdiAtg3KO and AdiAtg16L1KO mice fed either a normal chow diet (NCD) or high-fat diet (HFD) diet. Tamoxifen was administered in

concert with initiation of the dietary regimen. Depletion of Atg3 or Atg16L1 in adipocytes had no effect on body weight, weight gain, or adiposity under either the NCD or HFD conditions (Figures 1E–1H and S2A–S2C), nor did it alter whole-body energy expenditure, food intake, or physical activity (data not shown). Histological examination of epididymal white adipose tissue (eWAT) from NCD-fed mice revealed heterogeneity in adipocyte diameter and a slight reduction in adipocyte number (Figures 1I and 1J). BAT from AdiAtg3KO mice appeared less dense and contained more lipid vacuoles compared with BAT from wildtype mice (Figure S3F).

In obesity, adipose tissue becomes infiltrated with immune cells, such as macrophages, in a process that appears to mediate remodeling of adipose tissue (Sun et al., 2011) but also contributes to insulin resistance (Weisberg et al., 2003). Depletion of Atg3 in adipocytes led to massive inflammation of eWAT, even when mice were maintained on an NCD. This was evidenced by a 15-fold increase in the number of crown-like structures (Figures 1K and 1L), a 40% enhancement in F4/80 staining (Figures S1I and S1J), and induction of inflammatory gene expression (Figure 1M). However, despite enhanced adipose tissue immune cell infiltration, we found no difference in circulating tumor necrosis factor α (TNF-α), interleukin-6 (IL-6), or MCP1 between wild-type mice and AdiAtg3KO mice fed an NCD (Figures S1T–S1V). Furthermore, we did not detect any differences in F4/80-positive macrophages in the liver and gastrocnemius of wild-type and AdiAtg3KO mice fed an NCD or HFD (Figures S1O–S1R). Last, we also did not find any difference in circulating FGF21 between the groups (Figure S1S).

Depletion of Atg3 and/or Atg16L1 Induces Adipose and Systemic Insulin Resistance

We next assessed glucose homeostasis by performing glucose tolerance tests (GTTs) and insulin tolerance tests (ITTs) in AdiAtg3KO mice fed an NCD or HFD. AdiAtg3KO mice had impaired GTTs and ITTs under both NCD and HFD conditions compared with WT mice (Figures 2A–2D and S2J–S2M). The AdiAtg3KO mice had higher serum insulin (Table S1) and required more insulin to clear exogenously administered glucose (Figure 2E), further suggesting the development of peripheral insulin resistance. Similarly, AdiAtg16L1KO mice had impaired GTTs and ITTs compared with WT mice when fed an NCD (Figures S2D–S2G). The impairment in adipocyte autophagy led to increased hepatic gluconeogenesis, as evidenced by the increased circulating glucose produced following challenge with pyruvate (Figures S2N and S2O). Liver and muscle lipid accumulation, although enhanced by the HFD, was not significantly different between wild-type and AdiAtg3KO mice (Figures S1K–S1N). However, the size of the lipid droplets in the liver was reduced in AdiAtg3 KO mice compared with wild-type controls on an HFD.

To further investigate the relative contribution of fat, skeletal muscle, and liver in the observed insulin resistance, we injected animals with insulin and measured insulin-stimulated Akt phosphorylation (Ser473) in eWAT, BAT, liver, and skeletal muscle. As shown in Figures 2F–2J, insulin-stimulated phosphorylation of Akt was reduced in all tissues examined from the AdiAtg3KO mice compared with wild-type controls, suggesting that the absence of adipocyte autophagy caused peripheral insulin resistance. Moreover, insulin-stimulated 2-deoxyglucose uptake was severely impaired in eWAT explants from

NCD-fed AdiAtg3KO mice (Figure 2K). Together, these data suggest that post-development impairment of adipocyte autophagy caused insulin resistance independent of obesity.

Post-Developmental Depletion of Atg3 Led to Dysfunctional Mitochondria in Autophagy-Deficient WAT and BAT Adipocytes

The impairment in adipocyte autophagy led to dysfunctional mitochondria in both the WAT and BAT depots. The tricarboxylic acid (TCA) cycle enzyme aconitase and the mitochondrial chaperonin HSP60, markers of mitochondrial mass, were increased in both eWAT and BAT of AdiAtg3KO mice compared with wildtype controls (Figures 3A–3D). Furthermore, the accumulation of mitochondrial markers occurred despite a reduction in mRNA expression of indices of mitochondrial biogenesis, such as *Pgc1a, Pgc1b*, and *Tfam* in BAT and Pgc1b in eWAT of AdiAtg3KO mice (Figure S3H and S3I). These results suggest that mitochondria from autophagy-deficient adipocytes may not be cleared appropriately. Although the mitochondrial number was unchanged in BAT and eWAT of AdiAtg3KO mice, mitochondrial size increased in eWAT of AdiAtg3KO mice, suggesting increased swelling (Figures S3A–S3D). The above results were also confirmed using primary brown preadipocytes isolated from the interscapular region of $Atg3^{f/f}$ mice. The cells were allowed to fully differentiate before adenovirus-mediated infection with Cre-GFP or a GFP control was performed. We achieved about 70% and 80% knockdown of Atg3 mRNA and protein, respectively (Figures 3E–3H). Fully differentiated cells were treated with bafilomycin A1(Baf-A1, an inhibitor of autophagosome-lysosome fusion) to measure the autophagic flux and the accumulation of mitochondrial proteins. As depicted in Figures 3I and 3J, Baf-A1 treatment of GFP-infected control cells increased LC3I and LC3II proteins, suggestive of impaired lysosomal clearance of LC3II-associated autophagosomes. In contrast, Ad-Cre-infected cells exhibited a decrease in LC3II content at baseline and after Baf-A1 treatment, suggesting an impaired autophagic flux. Consistent with this observation, p62 accumulated only in Atg3-deficient adipocytes treated with Baf-A1 (Figure 3K). Atg3-deficient adipocytes had more acconitase and HSP60 protein content, especially when lysosomal clearance of autophagosomes was compromised (Figures 3L and 3M). Interestingly, eWAT from AdiAtg3KO mice exhibited enhanced mRNA expression of Bnip3, Bnip3l, and Pink1, positive regulators of mitochondrial autophagy, suggestive of an adaptive response aimed at mitigating mitochondrial impairments.

Depletion of adipocyte autophagy led to a profound alteration in mitochondrial morphology and impairment in mitochondrial function. Mitochondrial volume was enhanced and cristae were dispersed, suggesting mitochondrial swelling in BAT of AdAtg3KO mice (Figures S6B–S6D). Furthermore, pyruvatedriven oxygen consumption rates (OCRs) were diminished in BAT of AdiAtg3KO mice (Figure 3N). Similarly, the basal and maximal OCR and the compensatory increase in extracellular acidification rate (ECAR) after addition of oligomycin and 4-(Trifluoromethoxy)phenyl)hydrazono)malononitrile (FCCP) were completely abolished in eWAT and inguinal white adipose tissue (iWAT) of AdiAtg3KO mice (Figures 3O–3R). The defect in mitochondrial oxidative capacity may have participated in WAT and BAT dysfunction, as evidenced by reduced hormone-stimulated lipolysis in WAT and a blunted cold-induced thermogenesis in BAT of AdiAtg3 KO mice (Figures S3E–S3G). Together, these results demonstrate that autophagy is necessary for the maintenance of

mitochondrial function in mature adipocytes and that a failure in this process results in dysfunctional mitochondria.

Impairing Adipocyte Autophagy Induced Nrf2 and Keap1 Signaling in Adipose Tissue and Liver

To probe possible mechanisms leading to dysfunction of WAT and BAT when autophagy is impaired, we generated an unbiased profile of transcripts in eWAT from AdiAtg3KO and control mice. We found that loss of Atg3 elicited a profound enrichment of gene sets associated with Nrf2 and Keap1 signaling, a transcriptional network implicated in mediating anti-inflammatory and anti-oxidant responses (Figure 4A). Pathway analysis revealed an increase in xenobiotic and glutathione metabolism (Figure 4B), suggesting the induction of Nrf2 signaling. qRTPCR and western blotting confirmed that mRNA and protein expression of Nrf2, Keap1, and the Nrf2 targets heme oxygenase (Hmox1) and nicotinamide adenine dinucleotide phosphate (NAD(P)H) dehydrogenase quinone 1 (Nqo1) were enhanced in eWAT and BAT of AdiAtg3KO mice (Figures 4C–4H). Similar results were obtained when analyzing adipose tissue of AdiAtg16L1KO mice (Figures S4E–S4H). Transcripts encoding other detoxifying enzymes known to be regulated by Nrf2, such as the glutathione S-transferase 3 (Gsta3), were also elevated by 3- and 12-fold in eWAT and BAT of AdiAtg3KO mice, respectively (Figures 4I and 4J).

The mechanism linking impairments in adipocyte autophagy to enhanced Nrf2 and Keap1 signaling may involve accumulation of the scavenger protein p62. Under quiescent conditions, the ubiquitin-proteasome degrades Nrf2 through Keap1 (Cullinan et al., 2004). However, under stress conditions, the modification of cysteine residues on Keap1 leads to its inactivation (Dinkova-Kostova et al., 2002; Kobayashi et al., 2006). Thus, Nrf2 becomes stabilized and translocates to the nucleus to induce the transcription of numerous cytoprotective genes (Kobayashi and Yamamoto, 2006). The adaptor protein p62 has been shown to accumulate in autophagy-deficient liver cells, allowing it to interact with the Nrf2-binding site on Keap1, leading to stabilization of Nrf2 (Komatsu et al., 2010). Consistent with this finding, we observed a substantial accumulation of p62 in eWAT and BAT of AdiAtg3KO and AdiAtg16L1KO mice (Figures 1A–1D and S1E–S1H) and in Atg3-deficient adipocytes after treatment with Baf-A1 (Figure 3K). Nonetheless, we cannot rule out the possibility that oxidative modifications on Keap1 prevented its degradation by the proteasome. Indeed, we observed a parallel increase in Keap1 protein expression in eWAT of AdiAtg3KO mice (Figures 4E and 4G). The most unexpected finding in the current study is that we observed a similar induction of Nrf2 and Keap1 signaling in liver but not skeletal muscle obtained from AdiAtg3KO mice (Figures S4A–S4D). Below we discuss potential mechanisms driving this adipose-liver crosstalk mechanism.

Deficiency of Adipocyte Autophagy Reveals Crosstalk between Fat and Liver Mediated by HDL-Transported Lipid Peroxides

Nrf2 signaling is involved in the detoxification of electrophilic molecules and reactive aldehydes. Thus, we reasoned that impairment of autophagy might lead to the accumulation of lipid peroxides in the adipose depots. Application of two independent methods to measure lipid hydroperoxides (LPOs) and one of their derivative products, thiobarbituric acid-

reactive substances (TBARSs), confirmed that this was the case. LPO and TBARS levels were elevated in WAT, BAT, and serum from AdiAtg3KO mice (Figures 4K–4O). Consistent with increased adipose LPO levels, 4-hydroxynonenal-modified protein adducts were elevated in eWAT of AdiAtg3KO mice (Figures S4J and S4K).

The increase in LPOs was not restricted to adipose tissue of AdiAtg3KO mice because we also found that these species reached the liver and the muscle (Figures S4L and S4M). We similarly found that LPO levels were increased in the serum of AdiAtg16L1KO mice (Figure S4I). To determine what component of serum is responsible for carrying and transmitting LPOs systemically, we measured the LPO content in chromatographic fractions of serum. Remarkably, we found that the majority of circulating LPOs produced in adipose tissue of AdiAtg3KO and AdiAtg16L1KO mice resided in HDL particles (Figures 4P, S4O, and S4P). We further assessed the activity of the HDL-associated esterase paraoxanase (Pon1), an HDL-associated esterase that appears to contribute to the antioxidant and anti-atherosclerotic capabilities of HDL but that itself is inhibited when excess oxidized lipids accumulate in HDL particles (Getz and Reardon, 2004; Litvinov et al., 2012). Consistent with pathologic accumulation of lipid peroxides in HDL, paraoxanase activity was indeed reduced in the serum of AdiAtg3KO mice (Figure S4N).

These data present the provocative hypothesis that lipid peroxides or other reactive aldehydes produced in adipose tissue might themselves mediate inter-tissue communication between adipocytes and liver, potentially communicating the extent of adipose tissue damage to the liver and activating detoxification pathways in both organs. To explore the feasibility of this mechanism, we tested whether LPOs produced by adipocytes and reconstituted with hepatocytes *in vitro* are sufficient to replicate activation of Nrf2. We treated differentiated 3T3-L1 adipocytes with a lipid peroxide generator, tert-butyl hydroperoxide (tBHP); the cells were washed to remove any persistent tBHP and then incubated for 24 hr in fresh medium to produce conditioned medium (CM). Adipocytes treated with tBHP released 4-fold more LPOs into the medium than untreated adipocytes (Figure 4Q), and the CM of tBHP-treated adipocytes was sufficient to significantly increase Nrf2, Keap1, and Nqo1 protein expression in hepatocytes relative to the CM of untreated adipocytes (Figures 4R and 4S).

These studies reveal that insufficient autophagy within mature adipocytes impaired mitochondrial function and accumulation of lipid peroxides. These adipose-specific changes were sufficient to alter liver and muscle insulin sensitivity and whole-body glucose homeostasis, proving sufficient to drive the metabolic abnormalities that contribute to diabetes and heart disease. A surprising contributing mechanism was the lipid peroxides themselves, which trafficked through HDLs to the liver and were capable of eliciting robust changes in signaling in hepatocytes. These findings suggest a mechanism that contributes to the systemic metabolic impairments resulting from adipose damage. In addition, because alterations in quality and function of high density lipoprotein-cholesterol (HDL-C) have been associated with CVD risk even when HDL-C levels are normal, these findings point to a potential mechanism by which adipose tissue dysfunction can promote CVD.

Prior studies investigating the role of autophagy in adipose tissue have relied on KO of key components of the autophagic machinery in early stages of development, before formation of adipose tissue. For example, genetic KO of Atg7 controlled by the *Fabp4-Cre* recombinase resulted in impaired white and brown adipocyte differentiation and a compensatory increase in beige adipocytes in inguinal fat, leading to leanness and enhanced insulin sensitivity during high-fat feeding (Singh et al., 2009a; Zhang et al., 2009). These important findings are likely explained by the emerging roles for autophagy in adipocyte differentiation. Furthermore, these prior studies could not explain the increased mortality in *Fabp4-Cre*-AtgKO mice despite a favorable metabolic profile (Singh et al., 2009b; Zhang et al., 2009). We believe that this mortality was the result of Atg7 deletion in the CNS because *Fabp4-Cre* mice also express *Cre* recombinase in non-adipose tissues such as the CNS (Harno et al., 2013). Indeed, deletion of autophagy in the CNS through KO of Atg7 or Atg5 resulted in increased mortality (Kuma et al., 2004), again demonstrating that the use of *Fabp4-Cre*-mediated deletion of autophagy is non-specific to adipose tissue, a conclusion supported by several recent reports (Jeffery et al., 2014; Martens et al., 2010). Nonetheless, the results obtained in those excellent studies are in stark contrast to those reported here, where post-differentiation depletion of the autophagic machinery elicited profound impairments in metabolic homeostasis. Moreover, post-differentiation depletion of the autophagic machinery did not alter total lipids, as assessed by oil red O staining (data not shown), but we cannot exclude the possibility that lipid mobilization in response to a stimulus maybe affected in autophagy-deficient adipocytes. Finally, we did not observe an increase in beige adipocyte number as visualized by histology or by UCP1 expression. Thus, our work reveals a distinct and separable role for autophagy in mature adipocytes.

We suggest that autophagy may be involved in the maintenance of proper mitochondrial function and the prevention of lipid peroxidation production. We also cannot exclude a role for autophagy in the elimination of oxidized lipids through lipophagy. For these reasons, even though certain markers of autophagy are increased in adipose tissue of obese humans, it is possible that this response is compensatory in nature and that autophagy is not sufficiently functional to protect adipocytes from injury because both mitochondrial dysfunction and lipid peroxidation occur in adipose tissue with obesity (Boudina and Graham, 2014; Ferhat et al., 2018). Consistent with this possibility, a recent study showed that autophagic flux is decreased in adipocytes from obese humans and animals (Soussi et al., 2015)

A compelling finding of this work was the identification of lipid peroxides as signaling entities that could participate in adipose-muscle or adipose-liver crosstalk. In particular, this study presents the compelling hypothesis that these metabolites or other oxidized lipid species might traffic to other tissues as a means to communicate adipose tissue damage. Indeed, prior studies have shown that lipid peroxides such as 4-hydroxynonenal (4-HNE) are elevated in humans and in animal models with obesity and type 2 diabetes and can directly impair insulin signaling and glucose uptake in muscle and in preadipocytes *in vitro* (Demozay et al., 2008; Pillon et al., 2012). These effects could be reversed by the use of a glutathione precursor such as N-acetyl cysteine (NAC), suggesting the involvement of oxidative stress in this process.

Future studies using mitophagy reporter mice will be necessary to find out whether ablation of adipocyte autophagy is required for the elimination of dysfunctional mitochondria and the precise mechanisms by which lipid peroxides or other reactive lipids modulate liver metabolism and insulin sensitivity.

STAR⋆METHODS

CONTACT FOR REAGENT AND RESSOURCE SHARING

Further information and requests for resources and reagents should be directed to and will be fulfilled by the Lead Contact, Sihem Boudina (Sihem.boudina@u2m2.utah.edu).

EXPERIMENTAL MODEL AND SUBJECT DETAILS

Mice were maintained under standard laboratory conditions at a temperature of 22 ± 2C, relative humidity of 50 ± 5% and photoperiod of 12h (12hdark and 12h-light cycle). All animal experiments were performed according to procedures approved by University of Utah Institutional Animal Care and Use Committee and adhered to NIH standards. Experimental mice were individually caged and only male mice were used for the experiments. The ages of all mice used in the studies are as indicated in figure legends. Littermates of the same sex were randomly assigned to experimental groups. Animal weight are reported in figures and supplemental figures. All animals were used in scientific experiments for the first time. This includes no previous exposures to pharmacological substances. High fat diets were provided to the indicated mice to induce obesity. Health status was normal for all animals.

A total of 238 adult male mice were used. Stain details and number of animals in each group are as follows: 29 $Atg3^{fl/fl}$ mice; 37 $Atg16L1^{fl/fl}$ mice; 58 Adipoq-$pCreER^{T2}$; 77 AdiAtg3KO mice and 37 AdiAtg16L1KO mice.

METHOD DETAILS

Animal Studies—Atg3 and Atg16L1 floxed mice were generated from targeted C57BL/6 embryonic stem (ES) cells that were obtained from the European Conditional Mouse Mutagenesis Consortium ($Atg3^{tm1a(EUCOMM)Hmgu}$ and $Atg16L1^{1tm1a(EUCOMM)Wtsi}$) at University of Utah transgenic and gene targeting mouse core facility and crossed with Flp recombinase transgenic mice to remove LacZ and neomycin gene. Adipocytes-specific Atg3 and Atg16L1 KO mice were generated by crossing $Atg3^{fl/fl}$ or $Atg16L1^{fl/fl}$ mice with Adipoq$CreER^{T2}$ mice. Tamoxifen (1mg/day) was administered i.p. every day for 5 days starting at 8 weeks of age. Briefly, Tamoxifen was dissolved at 10mg/ml in corn oil at 37°C. Animals were injected i.p. with 100 μl Tamoxifen/day for 5 consecutive days. Tamoxifen-injected mice were sacrificed after 12 weeks of either normal chow or high fat feeding. The first Tamoxifen injection started along with the designated diet.

Histology and Morphometry—Epididymal (eWAT) depot and interscapular brown adipose tissue (BAT) were fixed in 4% paraformaldehyde for 48 hr, embedded in paraffin, cut into 5-mm sections, and stained with Hematoxylin and Eosin (H&E). The total number of adipocytes was measured using the CellSens Software (Olympus). Adipocyte number per

area was averaged from at least 500 adipocytes counted from 12–15 images per animal. Crown-like structures were counted on paraffin-embedded and H&E stained eWAT sections. Paraffin-embedded eWAT sections were stained with an anti-F4/80 antibody to detect macrophages in the adipose tissue. The images were acquired with an XM10 Olympus fluorescent camera (Olympus). F4/80 immunofluorescence staining was quantified based on color intensity using the CellSens Software (Olympus) in representative nonconsecutive fields per slide from three slides per animal in a blinded fashion.

Western Blot Analysis—WAT was solubilized in lysis buffer containing 18 mM CHAPS, 10 mM Tris and 1mM EDTA with protease and phosphatase inhibitor cocktail (Thermo Fisher Scientific). All other mouse tissues were solubilized in RIPA lysis buffer containing10 mM Tris-HCl, pH 7.4, 5 mM EDTA, 5 mM EGTA, 150 mM NaCl, 10% glycerol, 1% NP-40, 0.5% Triton X-100 and protease inhibitors. Protein concentration was measured using a BCA protein assay kit (Pierce). Proteins were loaded to Novex NuPAGE Bis-Tris Gels (Invitrogen), transferred to nitrocellulose membrane by using iBlot gel transfer device (Invitrogen), and probed with specific primary antibodies followed by HRP-conjugated secondary antibodies. Bands were detected by using chemiluminescence with GENE Gnome (Syngene Bio imaging) and analyzed by GeneTools (Syngene Bio imaging).

Insulin, Glucose and Pyruvate Tolerance Tests—Mice were fasted 4 hr (for ITT) or 6 hr (for GTT) respectively starting in the morning (8–9am). Baseline (fasting) blood glucose was measured before insulin or glucose administration from venous blood via a small tail tip cut. Insulin (1U/kg body weight) (ITT), Glucose (2 g/kg body weight) (GTT) or pyruvate (2 g/kg body weight) (PTT) was injected i.p. Blood glucose values were obtained at 15 30, 60, 90 and 120 min from the initial tail cut.

Glucose Uptake—Epididymal white adipose tissue explants (20mg) were washed twice and incubated in DMEM/0.1% FA free BSA for 2 hr at 37C. Medium was removed and explants were washed twice in Krebs-Ringer HEPES (KRH) buffer containing 0.1% FA free BSA (pH 7.4) kept at 37C. Explants were incubated in 0.5 mL KRH buffer with either 0 or 100 ng/ml insulin for 10 min at 37C under 5% CO2. 100uM 2-deoxyglucose and 0.5 mCi/ml [^{3}H]-2-deoxyglucose were then added to the explants and incubated 20 min at 37C. Following incubation explants were dunked in ice-cold PBS buffer to stop transport and washed three times with PBS buffer in order to remove unbound label. Explants were lysed with RIPA buffer. ^{3}H radioactivity were determined by scintillation counting using a LS 5000 TD liquid scintillation system (Beckman). Basal glucose uptake was taken as 2-deoxyglucose uptake in the absence of insulin.

Mitochondrial Function—Mitochondrial function was assessed using the XF24 Flux analyzer (Agilent). Briefly, oxygen consumption rates (OCR) and extracellular acidification rates (ECAR) were assessed using freshly isolated mouse BAT, iWAT and eWAT. The tissue was rinsed with non-buffered KHB media containing 111 mM NaCl, 4.7 mM KCl, 2 mM MgSO4, 1.2 mM Na2HPO4, 0.5 mM carnitine and 2.5 mM glucose; they were then cut into pieces (~10 μg) and washed extensively. Then, each piece was placed into a single well of an XF24 Islet plate (Agilent) and covered with a customized screen that allowed free perfusion

while minimizing tissue movement. KHB buffer was added to each well, and OCR was measured. For BAT, basal respiration was first measured and then pyruvate (5 μM) was added as substrate. For WAT, basal respiration was recorded before oligomycin (10 μM) was added to inhibit ATP synthesis. FCCP (20 μM) was then supplied to artificially uncouple the mitochondria. Rotenone (3 μM) and Antimycin A (12 μM) were added simultaneously to inhibit complexes I and III of the electron transport chain respectively.

Electron Microscopy—BAT and eWAT samples were analyzed by electron microscopy, and mitochondrial size and number were determined by stereology in a blinded fashion using the point counting method.

Lipolysis—Fasted (6 hr) mice were used to measure lipolysis *in vivo* before and after injection of isoproterenol (10mg/g body weight, i.p.). Blood samples were collected at 0 and 15 min after isoproterenol injection and serum glycerol level was measured using a glycerol assay kit (Sigma).

Cold Tolerance Tests—Individual mice were placed in a 4°C cold room for 3 h in the absence of food in a cage. Body temperature was independently measured at 0 (right before entering the cold room), 60, 120 and 180 min after cold exposure using a rectal probe (Thermo Fisher).

Gene Expression and RNaseq Analysis—Total RNA was extracted by using the RNeasy lipid tissue RNA mini kit (QIAGEN). cDNA was synthesized from DNase I treated total RNA (2 μg) using VersoTM cDNA kit (Thermo Scientific). Random hexamers and Oligo(dT) primers were used to prime the cDNA synthesis. The synthesis was completed in accordance with manufacturer's instructions. The resulting cDNA was stored at 20°C for qRT-PCR. Quantitative PCR reactions were performed on the ABI7000 platform with FastStart Universal SyberGreen ROX kit (Roche). All reactions were completed in triplicate. Each 20 μl PCR reaction contained 0.05 to 0.1 μg cDNA, 2 × SYBR-Green Master Mix, and primers diluted to a final concentration of 0.4 μM. The cycling parameters were: 95°C for 15 min, 40 cycles of 95°C for 15 s and 60°C for 1 min. A melting curve was performed each primer pair at 0.1°C intervals between the temperatures of 60C and 95C.

For RNaseq analysis, samples were sent to University of Utah genomics core facility, evaluated by NanoDrop spectrophotometer reading and Agilent Bioanalyzer RNA 6000 chip for quality control, sequenced by Illumina HiSeq2000 with 50 cycle paired end sequencing. Data were analyzed by bioinformatics analysis service from the microarray core facility at the University of Utah. The criteria for differential expression included only genes with a FDR of < 0.05 or log-transformed false discovery rate (FDR) of > 13 and with a fold change greater than or equal to ± 1.5 relative to controls. The Fragments Per Kilobase Million (FPKM) values of the differentially expressed genes (DEGs) were log-transformed and normalized to the average of the controls. These values were used to produce hierarchical clustering and generate heatmaps of the genes using Cluster 3.0 and Java Tree View open source programs, respectfully. The normalized log transformed FPKM values of the entire dataset were used to perform principal components analysis (PCA). We identified pathways that were significantly altered in AdiAtg3KO mice using the Database for Annotation,

Visualization, and Integrated Discovery (DAVID) software. Cell relevant, non-redundant Kyoto Encyclopedia of Genes and Genomes (KEGG) and Gene Ontology (GO) pathways or classifications in which the DEGs were enriched at a significance level of p % 0.05 were selected for display.

Lipid Peroxidation Assays—Lipid peroxidation products were analyzed by two separate assays. Lipid hydroperoxides assay kit (Cayman Chemical) was used to measure the formation of highly reactive and unstable hydroperoxides of both saturated and unsaturated lipids. Briefly, 200ul serum or 10mg homogenized tissue samples were mixed with equal volume extract R saturated methanol and two volume of cold chloroform. Samples were centrifuged at 1500 g for 5 min at 0°C. The bottom chloroform layer was collected and used for assay. The chloroform-methanol solvent (degassed, 2:1, 450ul) was added to 500ul of chloroform extract followed by addition of 50ul chromagen and incubation at room temperature for 5 min. The absorbance was measured at 500 nm. Methanol and chloroform need to be degassed on ice before the treatment. In addition to LPO, we measured thiobarbituric acid reactive substances (TBARS) that results from the reaction of the decomposition product of lipid peroxide malondialdehyde (MDA) with thiobarbituric acid using a colorimetric assay kit from Cayman Chemical following the manufacturer instructions.

Tert-butyl hydroperoxide (tBHP) Treatment—3T3-L1 preadipocytes were differentiated into adipocytes adipogenic differentiation media (DM) containing 10 mg/ml insulin, 0.25 mg/ml dexamethasone and 0.5 mmol/L isobutylmethylxanthine (IBMX) in DMEM-F12 with 10% FBS and 1% penicillin/streptomycin for 3 days. Cells were then maintained in DMEM-F12 with 10% FBS and 1% penicillin/streptomycin and 10 mg/ml insulin for 3 more days until lipids are formed. Cells were then treated with 100 mM tBHP or PBS for 24h. Cells were washed with fresh media and incubated for 24h. Rat hepatoma H4IIE cells were incubated for 6h in media collected from 3T3-L1 adipocytes treated with tBHP or PBS before proteins were extracted.

Paraxonase Activity—The organophosphatase activity of paraxonase was measured in serum using a fluorometric assay from Thermo Fisher Scientific according to the manufacturer instructions.

Lipoproteins Fractionation—HDL, LDL and VLDL Lipoproteins were isolated from serum of mice by fast liquid chromatography (FPLC). Briefly, biologic DuoFLow chromatography system (Bio-Rad) equipped with Superdex 200 10/300 column (GE Healthcare Life Sciences) was used with PBS as a running buffer. 200ul serum sample was loaded and collected by BioFrac fraction collector (Bio-Rad). Each fraction was verified by western blotting of apo A-1 for HDL receptors and apo B100 for LDL receptors.

Primary White Adipose Progenitors (APCs) Isolation, Transfection and Differentiation—Primary APCs from $Atg3^{fl/fl}$ mice were isolated from inguinal white adipose tissue and sorted by flow cytometry. Sorted APCs were seeded at 50,000/cm^2 in GM and cultured for 3 days without changing the media. At 100% confluence (3–4 days), the cells were exposed to adipogenic differentiation media (DM) containing 10 μg/ml insulin,

0.25 μg/ml dexamethasone and 0.5 mmol/L isobutylmethylxanthine (IBMX) in DMEM-F12 with 10% FBS and 1% penicillin/streptomycin. Undifferentiated or differentiated (3 days post-differentiation) APCs were treated with Ad CMV Cre-RSV eGFP or Ad CMV eGFP (Kerafast, Inc., Boston, MA) to delete Atg3 either before or after differentiation. APCs were switched to GM and cultured for 3 more days before staining neutral lipids with Oil Red O.

Primary Brown Adipose Tissue (BAT) Preadipocytes Isolation, Differentiation and Transfection—Fresh primary brown adipose tissue (BAT) preadipocytes were harvested from 6–8 days old *Atg3*$^{fl/fl}$ mice, cultured and differentiated post-confluency. Briefly, interscapular BAT was surgically isolated from young mice and instantly digested enzymatically for 1.5 hr in a 37C water bath using DMEM (11995–065, Invitrogen) supplemented with 10% fetal bovine serum (FBS) (FBS-BBT-5XM, RMBIO), 5% penicillin/streptomycin (PS) (15140122, Invitrogen), 20 mg/mL fatty acid-free bovine serum albumin (BSA) (A7030, Sigma-Aldrich) and containing 1 mg/mL Collagenase from *Clostridium hitolyticum* (C6885, Sigma-Aldrich). After tissue digestion, samples were passed through a 100 mm sterile nylon-cell strainer (Fisher-Scientific) and centrifuged at 700 g for 5 min. The cell pellet was then washed twice with DMEM (D5796, Sigma-Aldrich) supplemented with 10% FBS, 5% PS, 1X non-essential aminoacids (11140050, GIBCO), 1X Glutamax (35050061, Invitrogen), 1M HEPES (15630–080, Life technologies) and 0.1 mM b-mercaptoethanol. After centrifugation, the cell pellet containing the BAT preadipocytes were resuspended, seeded in a 12-well plate (1 well/sample) and incubated at 37°C, 5% CO_2. Media was replaced every two days until they reach 90%–100% confluency. After reaching confluency, BAT preadipocytes were differentiated to adipocytes using DMEM (11995–065, Invitrogen) supplemented with 10% FBS), 5% PS, 20nM insulin (I1882, Sigma-Aldrich), 0.5 μM dexamethanose (D1756, Sigma-Aldrich), 0.5 mM 3-Isobutyl-1-methylxanthine (IBMX) (I5879, Sigma-Aldrich), 1 nM 3,3′,5-Triiodo-L-thyronine sodium salt or T3 (T6397, Sigma-Aldrich) and 0.125 mM indomethacin (I7378, Sigma-Aldrich) for 48 hr. Differentiation media was then replaced by adipocyte maintenance media which contain 20 nM insulin and 1mM T3 in DMEM supplemented with 10% FBS, 5% penicillin/streptomycin. Maintenance media was replaced every two days until cells were ready for transfection. For adenovirus-Cre mediated Atg3 deletion, fully differentiated BAT adipocytes isolated from *Atg3*$^{fl/fl}$ mice were infected with adenovirus expressing eGFP (Ad CMV eGFP; FVQ002, Kerafast) or adenovirus expressing Cre-GFP (Ad CMV Cre-RSV GFP; FVQ005, Kerafast) using a PFU of 6.10^8/well, for two days before changing the media. After five days of infection, cells were treated with 0.1 μM of bafilomycin A1 (tlrl-baf1, Invivogen) for 24hours and thereafter determined RNA and protein expression of autophagy and mitochondrial proteins.

QUANTIFICATION AND STATISTICAL ANALYSIS

Data are presented as the mean ± SEM; $p < 0.05$ were considered significant. Student's t test was used to compare two independent groups. One-way or two-way ANOVA with Tukey post hoc test were used for multiple group analysis.

DATA AND SOFTWARE AVAILABILITY

The accession number for the RNaseq data reported in this paper is GEO: GSE120983.

Supplementary Material

Refer to Web version on PubMed Central for supplementary material.

ACKNOWLEDGMENTS

We thank Dr. Yong Hwan Han and Mrs. Tanya Forostyan for technical assistance. We thank Mrs. Nancy Chandler at the Electron Microscopy Core Facility at the University of Utah for help with acquiring EM images. We would like to thank Dr. Nina Wettschureck (University of Heidelberg, Heidelberg, Germany) for sharing the AdipoqCreER^{T2} mice. We would like to thank Mrs. Diana Lim for support while making the figures and illustrations. This work was supported by the United States National Institute of Diabetes and Digestive and Kidney Diseases (NIDDK) grants 1-R01-DK-098646-01A1 and R01-DK-099110 and the United States American Heart Association grant 16GRNT30990018 (to S.B.) and postdoctoral fellowship 15POST25360014.

REFERENCES

Boudina S, and Graham TE (2014). Mitochondrial function/dysfunction in white adipose tissue. Exp. Physiol 99, 1168–1178. [PubMed: 25128326]

Cullinan SB, Gordan JD, Jin J, Harper JW, and Diehl JA (2004). The Keap1-BTB protein is an adaptor that bridges Nrf2 to a Cul3-based E3 ligase: oxidative stress sensing by a Cul3-Keap1 ligase. Mol. Cell. Biol 24, 8477–8486. [PubMed: 15367669]

Demozay D, Mas JC, Rocchi S, and Van Obberghen E (2008). FALDH reverses the deleterious action of oxidative stress induced by lipid peroxidation product 4-hydroxynonenal on insulin signaling in 3T3-L1 adipocytes. Diabetes 57, 1216–1226. [PubMed: 18174527]

Dinkova-Kostova AT, Holtzclaw WD, Cole RN, Itoh K, Wakabayashi N, Katoh Y, Yamamoto M, and Talalay P (2002). Direct evidence that sulfhydryl groups of Keap1 are the sensors regulating induction of phase 2 enzymes that protect against carcinogens and oxidants. Proc. Natl. Acad. Sci. USA 99, 11908–11913. [PubMed: 12193649]

Ferhat M, Funai K, and Boudina S (2018).). Autophagy in Adipose Tissue Physiology and Pathophysiology. Antioxid. Redox Signal, Published online September 20, 2018 10.1089/ars. 2018.7626.

Fujita N, Itoh T, Omori H, Fukuda M, Noda T, and Yoshimori T (2008). The Atg16L complex specifies the site of LC3 lipidation for membrane biogenesis in autophagy. Mol. Biol. Cell 19, 2092–2100. [PubMed: 18321988]

Getz GS, and Reardon CA (2004). Paraoxonase, a cardioprotective enzyme: continuing issues. Curr. Opin. Lipidol 15, 261–267. [PubMed: 15166781]

Harno E, Cottrell EC, and White A (2013). Metabolic pitfalls of CNS Cre-based technology. Cell Metab. 18, 21–28. [PubMed: 23823475]

Jansen HJ, van Essen P, Koenen T, Joosten LA, Netea MG, Tack CJ, and Stienstra R (2012). Autophagy activity is up-regulated in adipose tissue of obese individuals and modulates proinflammatory cytokine expression. Endocrinology 153, 5866–5874. [PubMed: 23117929]

Jeffery E, Berry R, Church CD, Yu S, Shook BA, Horsley V, Rosen ED, and Rodeheffer MS (2014). Characterization of Cre recombinase models for the study of adipose tissue. Adipocyte 3, 206–211. [PubMed: 25068087]

Kirkin V, Lamark T, Sou YS, Bjørkøy G, Nunn JL, Bruun JA, Shvets E, McEwan DG, Clausen TH, Wild P, et al. (2009). A role for NBR1 in autophagosomal degradation of ubiquitinated substrates. Mol. Cell 33, 505–516. [PubMed: 19250911]

Kobayashi M, and Yamamoto M (2006). Nrf2-Keap1 regulation of cellular defense mechanisms against electrophiles and reactive oxygen species. Adv. Enzyme Regul 46, 113–140. [PubMed: 16887173]

Kobayashi A, Kang MI, Watai Y, Tong KI, Shibata T, Uchida K, and Yamamoto M (2006). Oxidative and electrophilic stresses activate Nrf2 through inhibition of ubiquitination activity of Keap1. Mol. Cell. Biol 26, 221–229. [PubMed: 16354693]

Komatsu M, Kurokawa H, Waguri S, Taguchi K, Kobayashi A, Ichimura Y, Sou YS, Ueno I, Sakamoto A, Tong KI, et al. (2010). The selective autophagy substrate p62 activates the stress responsive

transcription factor Nrf2 through inactivation of Keap1. Nat. Cell Biol 12, 213–223. [PubMed: 20173742]

Kosacka J, Koch K, Gericke M, Nowicki M, Heiker JT, Klo¨ ting I, Stumvoll M, Blu€her M, and Klo¨ ting N (2013). The polygenetically inherited metabolic syndrome of male WOKW rats is associated with enhanced autophagy in adipose tissue. Diabetol. Metab. Syndr 5, 23. [PubMed: 23668414]

Kuma A, Hatano M, Matsui M, Yamamoto A, Nakaya H, Yoshimori T, Ohsumi Y, Tokuhisa T, and Mizushima N (2004). The role of autophagy during the early neonatal starvation period. Nature 432, 1032–1036. [PubMed: 15525940]

Litvinov D, Mahini H, and Garelnabi M (2012). Antioxidant and anti-inflammatory role of paraoxonase 1: implication in arteriosclerosis diseases. N. Am. J. Med. Sci 4, 523–532. [PubMed: 23181222]

Martens K, Bottelbergs A, and Baes M (2010). Ectopic recombination in the central and peripheral nervous system by aP2/FABP4-Cre mice: implications for metabolism research. FEBS Lett. 584, 1054–1058. [PubMed: 20138876]

Mizushima N (2007). Autophagy: process and function. Genes Dev. 21, 2861–2873. [PubMed: 18006683]

Novak I (2012). Mitophagy: a complex mechanism of mitochondrial removal. Antioxid. Redox Signal 17, 794–802. [PubMed: 22077334]

Ost A, Svensson K, Ruishalme I, Brännmark C, Franck N, Krook H, Sandström P, Kjolhede P, and Strålfors P (2010). Attenuated mTOR signaling and enhanced autophagy in adipocytes from obese patients with type 2 diabetes. Mol. Med 16, 235–246. [PubMed: 20386866]

Pankiv S, Clausen TH, Lamark T, Brech A, Bruun JA, Outzen H, Øvervatn A, Bjørkøy G, and Johansen T (2007). p62/SQSTM1 binds directly to Atg8/LC3 to facilitate degradation of ubiquitinated protein aggregates by autophagy. J. Biol. Chem 282, 24131–24145. [PubMed: 17580304]

Pillon NJ, Croze ML, Vella RE, Soulére L, Lagarde M, and Soulage CO (2012). The lipid peroxidation by-product 4-hydroxy-2-nonenal (4-HNE) induces insulin resistance in skeletal muscle through both carbonyl and oxidative stress. Endocrinology 153, 2099–2111. [PubMed: 22396448]

Sassmann A, Offermanns S, and Wettschureck N (2010). Tamoxifeninducible Cre-mediated recombination in adipocytes. Genesis 48, 618–625. [PubMed: 20715175]

Singh R, Kaushik S, Wang Y, Xiang Y, Novak I, Komatsu M, Tanaka K, Cuervo AM, and Czaja MJ (2009a). Autophagy regulates lipid metabolism. Nature 458, 1131–1135. [PubMed: 19339967]

Singh R, Xiang Y, Wang Y, Baikati K, Cuervo AM, Luu YK, Tang Y, Pessin JE, Schwartz GJ, and Czaja MJ (2009b). Autophagy regulates adipose mass and differentiation in mice. J. Clin. Invest 119, 3329–3339. [PubMed: 19855132]

Sou YS, Waguri S, Iwata J, Ueno T, Fujimura T, Hara T, Sawada N, Yamada A, Mizushima N, Uchiyama Y, et al. (2008). The Atg8 conjugation system is indispensable for proper development of autophagic isolation membranes in mice. Mol. Biol. Cell 19, 4762–4775. [PubMed: 18768753]

Soussi H, Reggio S, Alili R, Prado C, Mutel S, Pini M, Rouault C, Clément K, and Dugail I (2015). DAPK2 Downregulation Associates With Attenuated Adipocyte Autophagic Clearance in Human Obesity. Diabetes 64, 3452–3463. [PubMed: 26038578]

Sun K, Kusminski CM, and Scherer PE (2011). Adipose tissue remodeling and obesity. J. Clin. Invest 121, 2094–2101. [PubMed: 21633177]

Weisberg SP, McCann D, Desai M, Rosenbaum M, Leibel RL, and Ferrante AW Jr. (2003). Obesity is associated with macrophage accumulation in adipose tissue. J. Clin. Invest 112, 1796–1808. [PubMed: 14679176]

Zhang Y, Goldman S, Baerga R, Zhao Y, Komatsu M, and Jin S (2009). Adipose-specific deletion of autophagy-related gene 7 (atg7) in mice reveals a role in adipogenesis. Proc. Natl. Acad. Sci. USA 106, 19860–19865. [PubMed: 19910529]

Highlights

- Post-developmental deletion of autophagy in adipocytes causes insulin resistance
- Mitochondrial dysfunction develops in autophagy-deficient adipocytes
- Enhanced Nrf2 and Keap1 signaling in autophagy-deficient adipocytes
- Crosstalk between fat and liver mediated by lipid peroxide-induced Nrf2 signaling

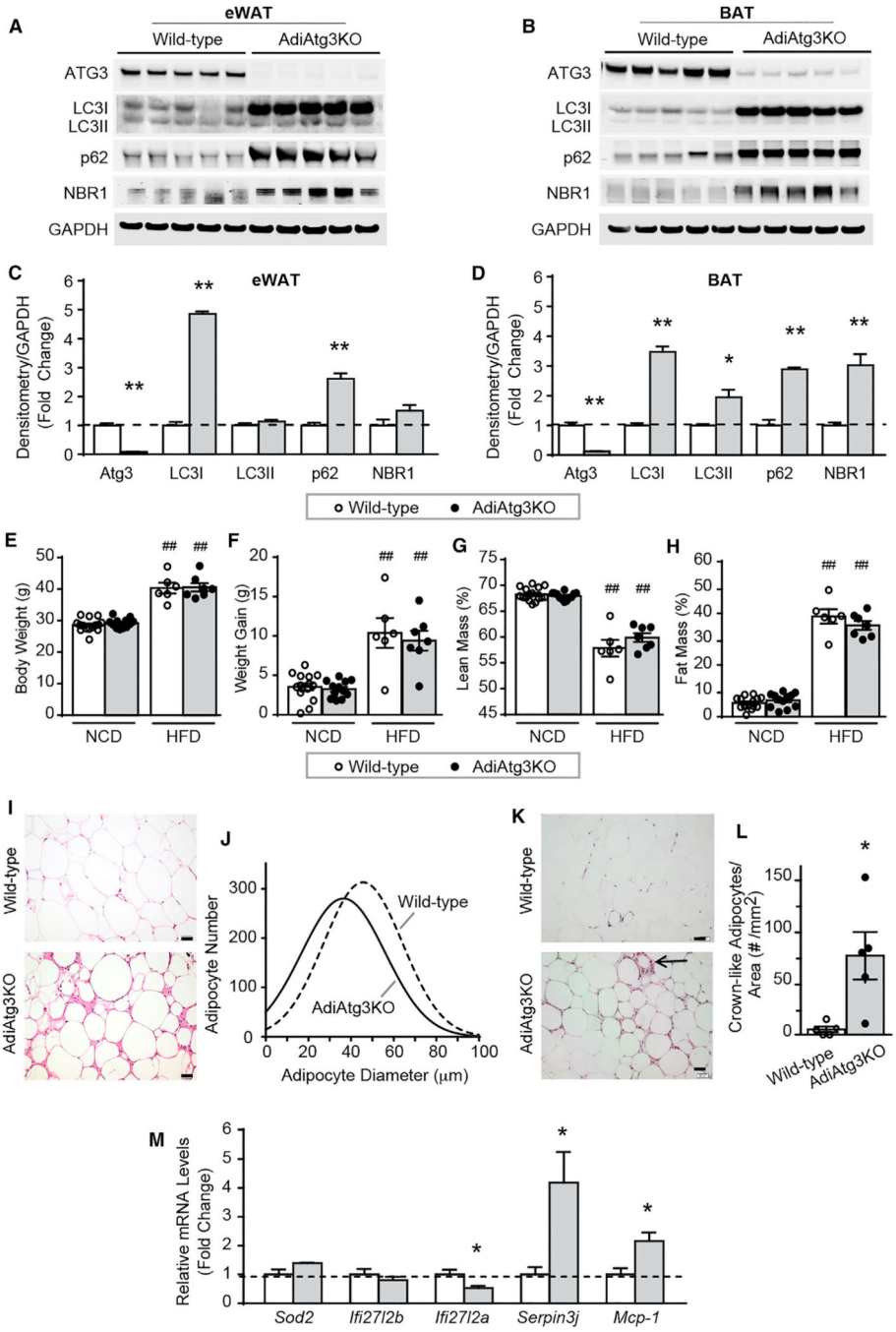

Figure 1. Post-Developmental Deletion of Adipocyte Autophagy Does Not Influence Adiposity but Causes Adipose Tissue Inflammation

(A and B) Western blot analysis of Atg3, LC3I, LC3II, p62, NBR1, and glyceraldehyde 3-phosphate dehydrogenase (GAPDH) in eWAT and BAT, respectively, from NCD-fed mice with the indicated genotypes.

(C and D) Densitometry of (A) and (B), respectively, normalized by GAPDH and expressed as fold change from wild-type (WT) controls.

(E–H) WT and AdiAtg3KO mice were fed an NCD or high-fat diet (HFD) for 16 weeks.

(E) Body weights.

(F) Weight gain.
(G) Percent lean mass.
(H) Percent fat mass.
(I and K) H&E staining of eWAT from NCD-fed mice with the indicated genotypes.
(J) Morphometric analysis of adipocyte number and diameter in eWAT from NCD-fed mice with the indicated genotypes.
(L) Morphometric quantification of crown-like structures in eWAT from NCD-fed mice with the indicated genotypes.
(M) Relative mRNA levels of inflammatory genes expressed as fold change from WT in eWAT from NCD-fed mice with the indicated genotypes.
Values are mean ± SEM (*$p < 0.05$, **$p < 0.005$ versus WT, ##$p < 0.005$ versus NCD of the same genotype); n = 5/group for (A)–(D) and n = 6–14/group for (E)–(M).

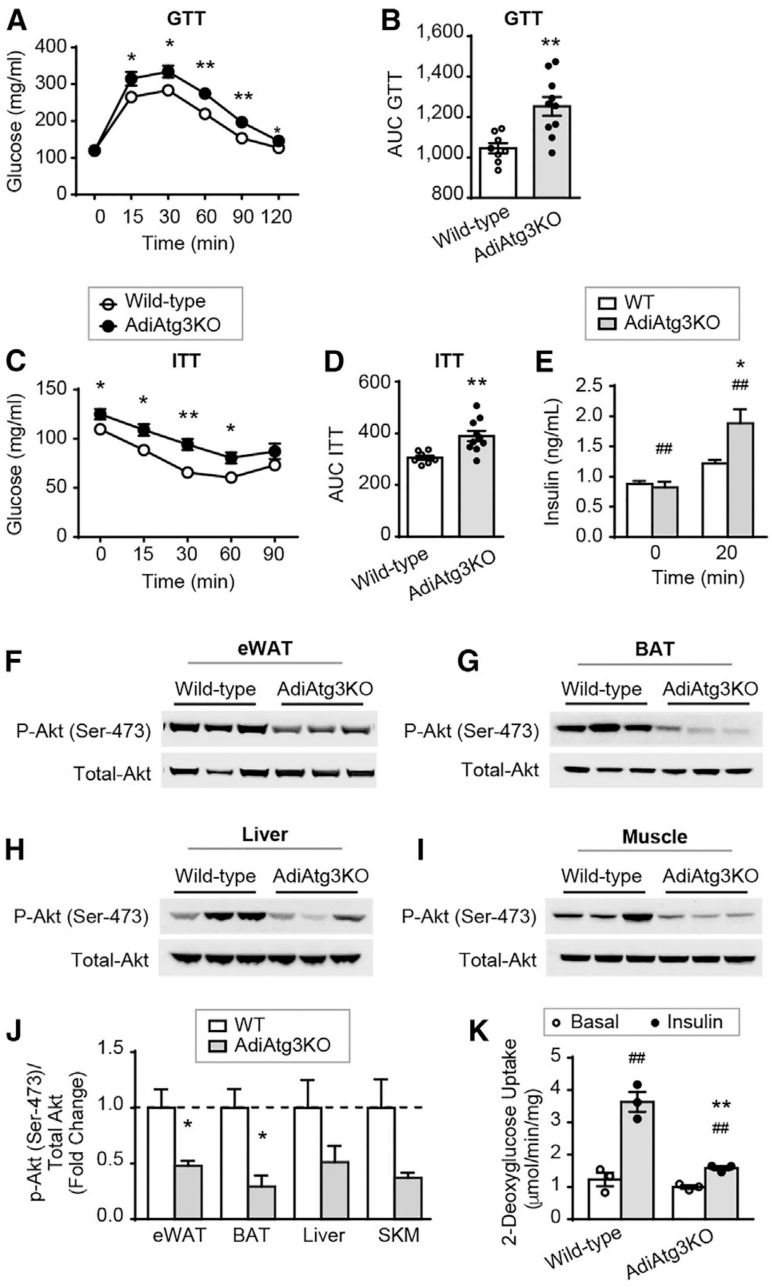

Figure 2. Deletion of Autophagy in Mature Adipocytes Causes Peripheral Insulin Resistance in AdiAtg3 KO Mice Fed a NCD

(A–K) WT and AdiAtg3 KO mice were fed an NCD for 12 weeks.

(A) Glucose tolerance tests (GTTs).

(B) Area under the curve (AUC) for GTTs.

(C) Insulin tolerance tests (ITTs).

(D) AUC for ITTs.

(E) Plasma insulin levels 0 and 20 min after glucose injection during GTTs.

(F–I) Western blot analysis of phospho-Akt (Ser473) and total Akt levels in eWAT, BAT, liver, and skeletal muscle from NCD-fed mice with the indicated genotypes.

(J) Densitometry of phospho-Akt to total Akt.

(K) Insulin-stimulated 2-deoxyglucose uptake in eWAT explants of NCD-fedmice with the indicated genotypes.

Values are mean ± SEM (*p < 0.05, **p < 0.005 versus WT, ##p < 0.005 versus basal). n = 8–10/group for (A)–(D), n = 6/group for (E), and n = 3/group for (F)–(K).

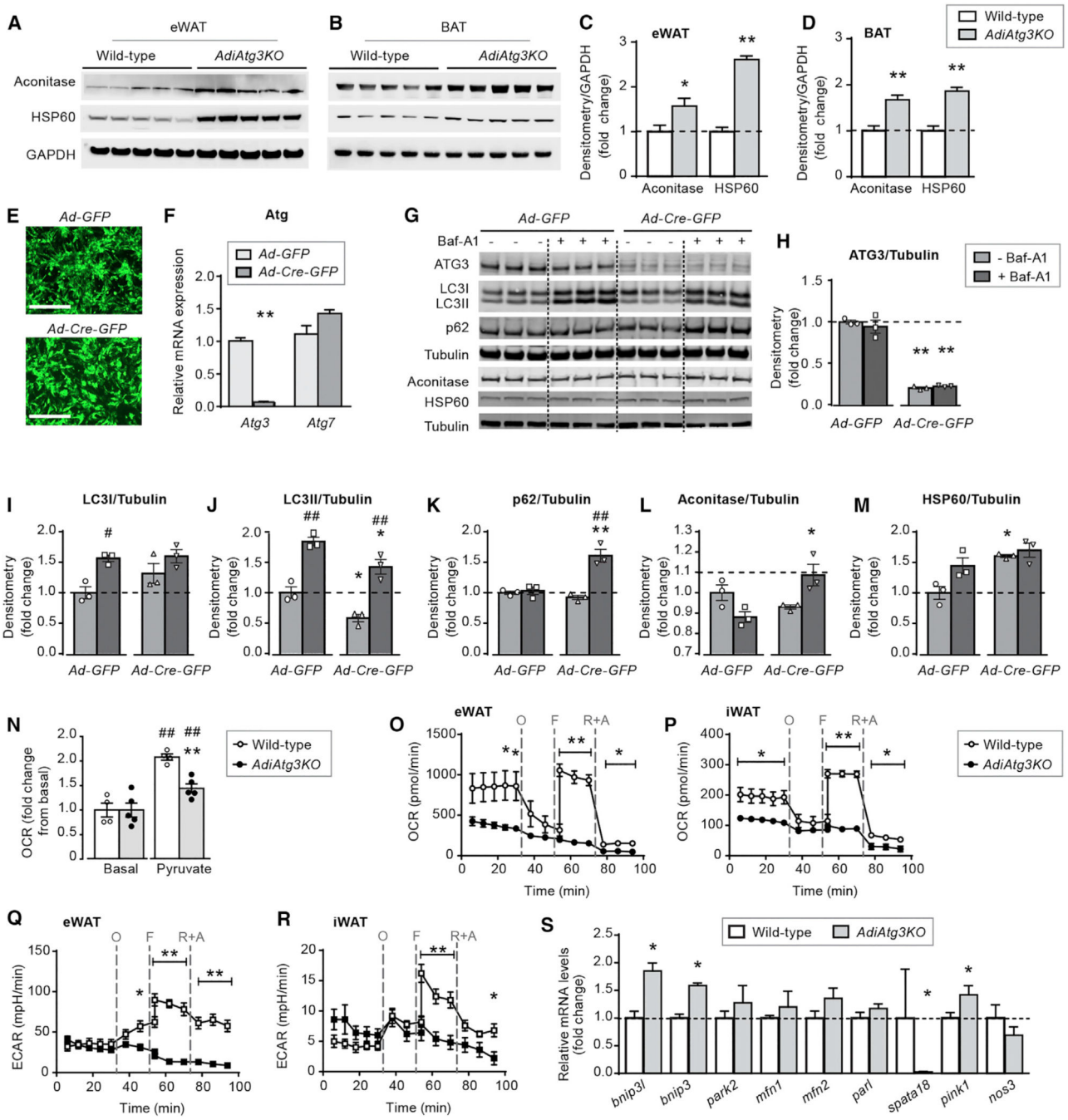

Figure 3. Accumulation of Dysfunctional Mitochondria Autophagy-Deficient White and Brown Adipocytes

(A–D and N–S) WT and AdiAtg3 KO mice were fed an NCD for 12 weeks.

(A and B) Western blot analysis of mitochondrial proteins (aconitase and HSP60) in eWAT and BAT, respectively.

(C and D) Densitometry of aconitase and HSP60 normalized by GAPDH and expressed as fold change from WT controls in eWAT and BAT, respectively. (E–M) Primary brown preadipocytes were isolated from the interscapular BAT of Atg3$^{f/f}$ mice and differentiated

for 3 days before being infected with adenovirus-Cre-GFP or adenovirus-GFP control. Cells were analyzed 6 days post-infection.

(E) Representative images of Ad-Cre-GFP- or Ad-GFP-infected cells 48 hr post-infection.

(F) Relative mRNA expression of Atg3 and Atg7 in Ad-Cre-GFP- or Ad-GFP-infected cells 4 days post-infection.

(G) Representative western blots of Atg3, LC3I, LC3II, p62, aconitase, HSP60, and tubulin in Ad-Cre-GFP- or Ad-GFP-infected cells 6 days post-infection. Cells were treated with saline or bafilomycin A1 (Baf-A1) for the last 24 hr.

(H–M) Densitometry of (G) normalized by tubulin and expressed as fold change from Ad-GFP control cells.

(N) Oxygen consumption rate (OCR) in BAT tissue sections.

(O and P) OCR in eWAT and iWAT tissue sections, respectively.

(Q and R) Extracellular acidification rate (ECAR) in eWAT and iWAT tissue sections, respectively.

(S) Relative mRNA levels of genes involved in mitochondrial clearance in eWAT.

Values are mean ± SEM (*$p < 0.05$, **$p < 0.005$ versus WT or Ad-GFP, #$p < 0.05$, ##$p < 0.005$ versus basal in (N) and versus without Baf-A1 in (I)–(K). n = 4–5/group for (A)–(D) and (N)–(S) and n = 3/condition for (E)–(M).

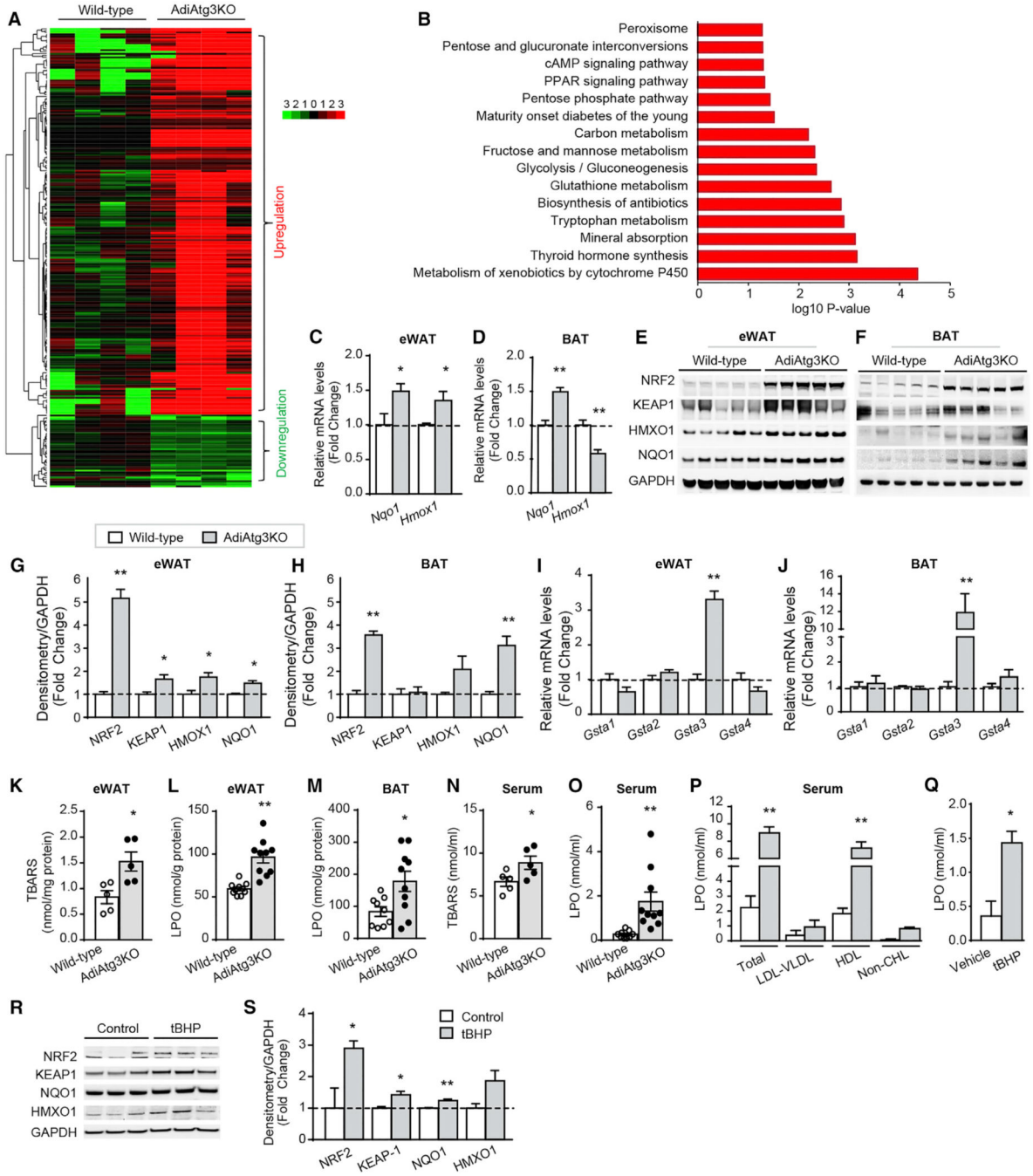

Figure 4. Autophagy Deletion in Adipocytes Enhances Nrf2 and Keap1 Signaling in Adipose Tissue and Causes Adipose and Systemic Elevation of Lipid Peroxides

(A–O) WT and AdiAtg3 KO mice were fed an NCD for 12 weeks.

(A) Heatmap showing hierarchical clustering of differentially expressed genes in AdiAtg3 KO mice. The FPKM (fragments per kilobase of exon per million reads mapped) values of individual samples were normalized to the average of WT controls.

(B) Kyoto Encyclopedia of Genes and Genomes (KEGG) pathway analysis showing the most upregulated pathways.

(C and D) Relative mRNA levels of the Nrf2 targets Nqo1 and Hmox1 in eWAT and BAT, respectively.

KEY RESOURCES TABLE

Rabbit anti-ATG3	Sigma-Aldrich	Cat# A3231; RRID: AB_1078235
Rabbit anti-LC3B	Sigma-Aldrich	Cat# L7543; RRID: AB_796155
Rabbit anti-ATG3	Cell Signaling Technology	Cat#3415S; RRID: AB_2059244
Rabbit anti-LC3	Cell Signaling Technology	Cat#2775; RRID: AB_915950
Rabbit anti-LC3B (D11) XP mAb	Cell Signaling Technology	Cat#3868; RRID: AB_2137707
Rabbit anti-Akt (Ser473) mAb	Cell Signaling Technology	Cat#4060; RRID: AB_2315049
Rabbit anti-Akt (pan) (C67E7) mAb	Cell Signaling Technology	Cat#4691; RRID: AB_915783
Rabbit anti-GAPDH (14C10)	Cell Signaling Technology	Cat#2118; RRID: AB_561053
Rabbit anti-HSP60 (D307)	Cell Signaling Technology	Cat#4870S; RRID: AB_2295614
Rabbit anti-Aco2	Cell Signaling Technology	Cat#6922S; RRID: AB_10828218
Mouse anti-NBR1 mAb (M01)	Abnova	Cat#H00004077-M01; RRID: AB_1016849
Mouse anti-SQSTM1/P62	Abnova	Cat#H00008878-M01; RRID: AB_437085
Mouse anti-4-HNE	Genox	Cat#MHN020P; RRID: AB_1106814
Rabbit anti-Heme oxygenase 1	Genetex	Cat#GTX101147; RRID: AB_1950502
Rabbit anti-NRF2	Genetex	Cat#GTX103322; RRID: AB_1950993
Rabbit anti-NQO1	Genetex	Cat#GTX100235; RRID: AB_1951017
Rabbit anti-KEAP1	Proteintech	Cat#10503–2-AP; RRID: AB_2132625
Rabbit anti-apoA-I	Santa Cruz	Cat#sc-30089; RRID: AB_2242716
Rabbit anti-apoB (S-18)	Santa Cruz	Cat#sc-11795; RRID: AB_2056951
Mouse anti-ATG16L	MBL	Cat#M150–3; RRID: AB_1278758
Ad CMV Cre – RSV eGFP	Kerafast, Inc.	FVQ005
Ad CMV eGFP	Kerafast, Inc	FVQ002
Human Insulin	Lilly	Cat HI-213
Tamoxifen	Sigma-Aldrich	Cat T5648
Tert-Butyl Hydroperoxide	Sigma-Aldrich	Car Cat 75–91-2
Bafilomycin A1	Invivogen	Cat Tlrl-baf1
Mouse Insulin ELISA	Crystal Chem	Cat 90080
Glycerol Assay Kit	Sigma-Aldrich	Cat MAK117
TBARS Assay Kit	Cayman Chemical	Cat 10009055
LPO Assay Kit	Cayman Chemical	Cat 705002
Paraxonase Activity Assay	Thermo Fisher Scientific	Cat E33702
RNaseq data	This study	GEO: GSE120983
Experimental Models: Cell Lines		
Primary white adipose tissue progenitors	This study	N/A
Primary brown adipose tissue preadipocytes	This study	N/A
Adipoq-pCreER^{T2} (B6)	Dr. Nina Wettschureck	N/A
Atg3$^{fl/fl}$ (B6)	This study	N/A
Atg16L1$^{fl/fl}$ (B6)	This study	N/A

AdiAtg3 KO (B6)	This study	N/A
REAGENT or RESOURCE	SOURCE	IDENTIFIER
AdiAtg16L1 KO (B6)	This study	N/A
Oligonucleotides		
Atg3 F GTACCTGACCCCGGTCCT	This study	N/A
Atg3 R TTGGACAGTGGACTAAGTG	This study	N/A
Recombinant DNA		
Graphpad Prism 7	Graphpad	https://www.graphpad.com/scientific-software/prism/
CellSens	Olympus	https://www.olympus-lifescience.com/en/software/cellsens/
GeneTools	Syngene Bioimaging	https://www.syngene.com/genetools/